# Photopatterning Crystal Orientation in Shape-Morphing Polymers

*Lindy K. Jang[1], Mustafa K. Abdelrahman[2], Taylor H. Ware[1,2]**

[1] Department of Biomedical Engineering, Texas A&M University, College Station, TX 77840, USA

[2] Department of Materials Science and Engineering, Texas A&M University, College Station, TX 77840, USA

KEYWORDS

Shape-morphing polymer, semicrystalline polymer, crystal alignment, photopatterning, smart polymer

ABSTRACT

Shape-morphing polymers have gained particular attention due to their unique capability of shape transformation under numerous external stimuli such as light, pH, and temperature. Their shape-morphing properties can be used in various applications such as robotics, artificial muscles, and

biomedical devices. To take advantage of the stimuli-responsive properties of the smart polymers in such applications, programming shape change precisely through a facile synthetic procedure is essential. Programmable shape morphing is readily obtained in hydrogels and liquid crystal polymer networks, but shape programming of semicrystalline polymers usually relies on low-resolution mechanical deformation. In this paper, a semicrystalline shape-morphing polymer with a controlled shape-programmability was developed via photopatterning crystal orientation using a spatially-controlled photopolymerization technique. The semicrystalline polymer network forms aligned crystallites at the boundaries between dark and bright regions during photopolymerization using a projector, which introduces anisotropic stimulus response in the films. The semicrystalline polymer films with photoaligned crystallites expand 9-15% in the direction perpendicular to the patterned lines when heated above the melting temperature. Furthermore, spatially patterning the crystal orientation enables the formation of various complex 3D structures including a helical coil, a coil with a handedness inversion, a cone, a saddle, and a twisting flower. Finally, the magnitude of the shape transformation was controlled by varying the polymerization temperatures, and the actuation temperature was tuned by changing the amount of crystallinity in the polymer films. The simplicity and ease of control of our approach to program complex 3D structures from 2D semicrystalline polymer films make it a promising system for the aforementioned applications.

## 1. INTRODUCTION

Shape-morphing polymers are capable of changing shape under external stimuli such as light, pH, temperature, electric field, magnetic field, and humidity.[1–5] Designing shape-morphing polymers that can form 3D structures under such stimuli have been intensively investigated for

their potential applications including smart packaging,[6] robotics,[7] artificial muscles,[8] and biomedical devices.[9,10] To achieve these applications, programming shape transformation in a controlled manner through a facile synthetic procedure is critical but remains challenging. As such, strategies to program shape morphing are of intense interest.

Various methods of programming shape change in polymeric films have been investigated. These methods can be classified by the stimulus that induces shape morphing, the thermomechanical properties of the shape morphing material, the reversibility of the shape change,[11] and the ability to pattern this shape morphing into complex forms.[12] For example, the swelling of a hydrogel can be controlled with patterned anisotropy[13] or with patterned magnitude,[14] resulting in low elastic modulus materials that morph into 3D forms. Similarly, the strain associated with order/disorder transitions in liquid crystal elastomers[15,16] and polymer networks[17] can be patterned. In both of these cases, shape typically changes with the applied stimulus and returns to the original form on removal of the stimulus.

To use the shape-morphing polymer film in the deformed state, irreversible shape transformations can be used. The most widely researched approach is to use the shape memory effect,[18,19] where strain in the structure is recovered in response to a stimulus. By controlling the amount of deformation[20,21] or the extent of recovery[22,23] of the shape memory polymer, the shape morphing can be patterned. Programming a temporary shape in a shape memory polymer can be done through complex mechanical deformation, but the material returns to the initial form in the presence of a stimulus. The ability to generate an irreversible shape transformation into a form that was never achieved by manufacturing might be useful in applications such as packaging, microsurgical tools, and self-deployable systems. For example, 3D printed shape memory polymers can be processed in such a way that local cure stresses are controlled,[24,25] resulting in

morphing to a new form on application of a stimulus. This process embeds the programming procedure into the manufacturing process, but it is not clear how to achieve such control in films that might be used in packaging, coatings, or as substrates for electronics.

Herein, we introduce a new route to program shape in a facile and controlled-manner in a semicrystalline polymer film via photopatterning crystal orientation using a spatially-patterned crosslinking technique. The semicrystalline polymer network is formed using thiol-ene click chemistry that simultaneously undergoes crystallization during photopolymerization.[26] By irradiating a visible light of a computer-generated dark and bright image into a monomer-filled cell, crystals are aligned at the boundaries of the dark and bright regions to build patterned anisotropic stress in the polymer network. After crosslinking is completed, the film adopts a flat shape dictated by the mold. However, when the polymer network undergoes a first order melting transition, anisotropic actuation is observed due to the release of the accumulated stress from the aligned crystals. This simple photopatterning technique allows one-pot synthesis and programming of shape-morphing polymer, spatio-selective actuation, and formation of complex 3D shapes, which broadens its potential to be used in various shape-morphing applications.

## 2. MATERIALS AND METHODS

### 2.1. Materials

1,7-Octadiene (OTD) and diallyl adipate (DAA) were purchased from Fisher Scientific. Pentaerythritol tetrakis(3-mercaptopropionate) (PETMP) and 1,9-nonanedithiol (NDT) were purchased from Sigma-Aldrich. Acetone and isopropyl alcohol (IPA) were purchased from

VWR. The photoinitiator, bis(2,4,6-trimethyl benzoyl)phenyl phosphine oxide (I-819), was donated by BASF Corporation. All chemicals were used as received.

## 2.2. Synthesis and photopatterning of semicrystalline films

Monomer solutions were prepared by adding equimolar amounts of alkenes (molar ratio of OTD:DAA = 75:25 or 50:50) to thiols (molar ratio of NDT:PETMP = 95:5) along with 3 wt% photoinitiator (I-819) as previously reported.[26] The solutions were heated to 70˚C with a heat gun, mixed thoroughly, and cooled at room temperature for 20 minutes. Glass slides (75 mm × 50 mm) were cleaned with a detergent (Alconox), rinsed (acetone, IPA and reverse osmosis (RO) water), and blow-dried. The cleaned glass slides were treated with water-repellent (Rain-x) on one side. Cells were prepared by placing two 25 μm spacers (polyimide film) between two water repellent treated glass slides and gluing them at the sides. The monomer solution was introduced into the cell using capillary action. A focused beam with a computer-generated dark and bright pattern was irradiated on one side of the cell for 30 seconds using a modified projector (Vivktek D912HD) with the UV filter removed and lenses repositioned to decrease the focal length. For samples polymerized at temperatures other than room temperature, a broadband dielectric mirror (Thorlabs Inc., NJ, USA) was used to reflect the projector image to irradiate the monomer-filled cell on either a hot plate or a Peltier plate (Meerstetter engineering GmbH, Rubigen, Switzerland). The same side of the film that was irradiated with the image generated by the projector was further cured with UV light (365 nm, OmniCure® LX400+, Lumen Dynamics) with an intensity of 6 mW/cm$^2$ for 10 minutes. The fabricated film was annealed at room temperature for at least 12 hours before characterization.

## 2.3. Polarizing optical microscopy

Polarizing optical microscope (POM; Olympus BX51, MA, USA) images were taken between crossed polarizers in transmission mode. To calculate the uniform birefringent area, we used Image J software to adjust the threshold and calculate the area of the lines showing the uniform birefringence.

## 2.4. Dimension change analysis

A polarizing optical microscope (POM; Olympus BX51, MA, USA) in bright field transmission mode was used to measure the dimension change of the films upon heating. Films were cut into small rectangular areas (0.2 – 1 $mm^2$) and placed on a glass slide within a drop of silicone oil. The glass slide with the film was placed on a thermal heat stage (Linkam Sci. Instr. LTD., Surrey, UK), and the heat stage was heated to 90˚C with a ramp rate of 50˚C/min. The change in dimension parallel and perpendicular to the patterned crystal lines were measured using Leica software. For the measurement of dimension change according to temperature, samples were placed on the thermal heat stage and heated to 90˚C with a ramp rate of 2˚C/min. Dimensions of the films were measured every 30 seconds using Leica software.

## 2.5. Differential scanning calorimetry

Thermal properties of the polymer films were analyzed using differential scanning calorimetry (DSC Q20, TA Instruments, DE, USA). Polymer samples (4-8 mg, n=3) were loaded into Tzero aluminum pans. Two heating cycles (–20 ~ 150˚C, ramp rate: 10˚C/min, 1 min equilibration after each ramp) were run, and the second heating cycle was used to obtain the melting temperature and the enthalpy of melt.

## 2.6. Dynamic mechanical analysis

For mechanical analysis of the polymer films, dynamic mechanical analysis (DMA, RSA-G2, TA Instruments, DE, USA) was performed. Samples (n=3) were prepared in rectangular strips (2 mm × 25 mm × 30 μm) with the ends gently wrapped using aluminum foil strips to prevent slipping. The foil-wrapped ends of the film strips were clamped at the tensile clamps. Storage moduli of samples were measured with an isothermal strain sweep (0.05 – 0.2%) at 1 Hz at room temperature. The storage moduli of the samples at 0.1% were used for comparison.

To measure thermomechanical properties, temperature sweep (25 – 100˚C) at 0.2% strain was performed using DMA with a heating ramp of 1˚C/min. Rectangular film samples (n=3) with dimensions of 5 mm × 25 mm × 100 μm were prepared. Each end was wrapped with an aluminum foil strip. Storage moduli were measured with 0.2 N preload and 100% force tracking. All samples for DMA analysis were stored under vacuum at least for 24 hours before testing.

## 2.7. Roughness measurement

Films with the OTD:DAA = 75:25 composition before and after heating to 90˚C were prepared on glass slides. The root-mean-squared roughness ($R_q$) of the films was measured using Bruker DektakXT Surface Profiler with a 2 μm stylus tip and a stylus tip force of 1 mg. Five scans of 500 μm lengths were conducted on each sample with a scan speed of 16.67 μm/s (n=3).

VEECO WYKO NT9100 Optical Profilometer was used with a VSI measurement type to obtain three-dimensional scan images of Control and the photopatterned films. Film samples before and after heating to 90˚C were scanned in 466.8 × 622.4 μm area.

## 2.8. Radius of curvature measurement

The OTD:DAA = 75:25 composition films with different UV crosslinking times at the front and back of the films were prepared. The monomer-filled cells were crosslinked with UV light (365 nm, OmniCure® LX400+, Lumen Dynamics) with an intensity of 6 mW/cm$^2$ for 10 minutes in total for the following conditions: 10 min front, 7.5 min front and 2.5 min back, 5 min front and 5 min back, and 2.5 min front and 7.5 min back. Rectangular strips (1 mm × 5 mm × 30 μm) were cut from the films and heated in a silicone oil bath at 90˚C. The curved strips were imaged at the side, and the radius of curvature was measured for each film strip by fitting a circle using Image J (n=3).

## 2.9. Statistical analysis

Uniform birefringent area, change in dimensions, and storage moduli were compared using Student's t-test. Values are presented as mean ± standard deviation.

## 3. RESULTS AND DISCUSSION

Programmable shape-morphing polymer films were fabricated by introducing regions of oriented crystallites. The semicrystalline polymer film was synthesized using a previously described synthetic approach. This material has the unique property of undergoing crystallization concurrently with photopolymerization.[26,27] Divinyl (OTD, DAA), dithiol (NDT), and tetrathiol (PETMP) monomers (**Fig. 1a**) were photopolymerized with the photoinitiator, I-819 by irradiating visible light patterns from a projector to photoalign crystal orientation. The schematic of the polymer network is shown in **Figure S1**. The monomer solution before photopolymerization does not show any birefringence when observed between crossed polarizers. However, upon photopolymerization with broadband light for 30 s, crystallites are formed, as evidenced by the formation of the birefringent area in the POM image (**Fig. 1b**). Using this concurrent crystallization and photopolymerization property of the polymer network, the crystal orientations in the polymer films are aligned by irradiating different patterns consisting of dark and bright regions through the projector, including lines inclined at 45˚ and Texas A&M University (TAMU) emblem (**Fig. 1b**). The aligned crystalline regions were formed at the boundaries between the dark and bright regions. We hypothesize that this orientation arises from the diffusion of monomers from the dark region to the bright region and/or the volume change associated with polymerization.[28–30] This hypothesis is further discussed below. As the monomers in the bright regions are photopolymerized and locked in the place, volume shrinks in

the bright regions as these regions crystallize.[29] Simultaneously, diffusion of monomers from the dark regions to the bright regions occurs perpendicular to the boundary between bright and dark regions.[31] Aligned lamellae form at the boundaries of the dark and bright regions as indicated by uniform birefringence in the POM images (**Fig. 2**). A 3D scan image of 1D1B film obtained from an optical profilometer shows that the bright region is thicker than the dark region in the film thickness, supporting that the diffusion occurred during photopatterning (**Figure S2**).

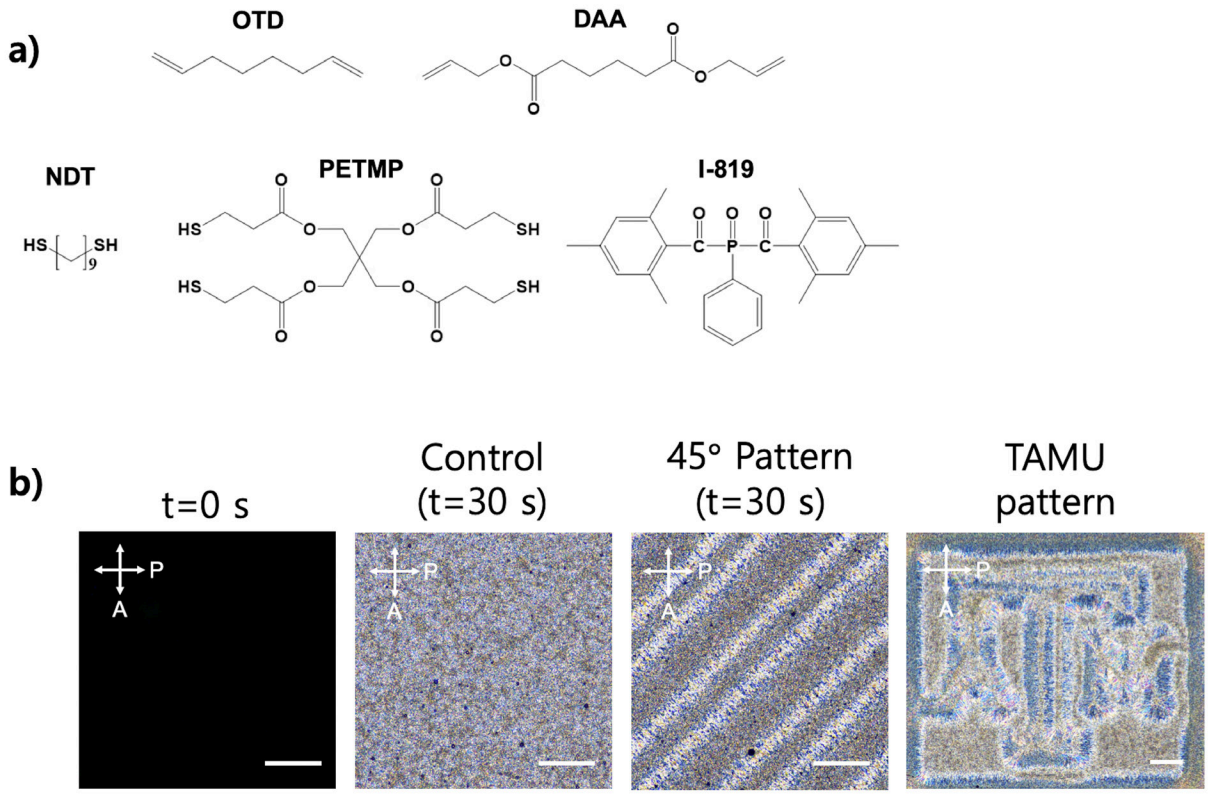


**Figure 1.** a) Chemical structures of monomers used in fabricating semicrystalline shape-morphing polymer films. b) POM images of samples between crossed polarizers (from left to right: monomer solution before photopolymerization, Control film photopolymerized with 30 s of broadband light, film photopolymerized with dark and bright striped patterns inclined at 45˚, film photopolymerized with Texas A&M University (TAMU) emblem image) (Scale bars: 200μm).

Striped patterns with different widths of dark and bright lines were used to introduce aligned crystal orientation in the semicrystalline films. Films were fabricated by irradiating three different photopatterns (1D2B, width of dark line: bright line = 1:2; 2D1B, width of dark line: bright line = 2:1; 1D1B, width of dark line: bright line = 1:1) on monomer-filled cells using a projector (**Fig. 2**). There was no significant difference in the widths of uniform birefringent lines that formed as a result of the three patterns, each showing birefringent lines of approximately 75-85 μm width (**Figure S3a**). It follows that the stresses generated at the boundary of dark and bright regions can be accommodated by orienting a similar area of material despite changes in the spacing of the interfaces. Due to the closer proximity of pattern lines for 1D1B, 1D1B films showed significantly larger uniform birefringent area per unit of film area than the other two patterns (**Figure S3b**). The 1D1B pattern line was the narrowest pattern that could be achieved without compromising resolution through the projector used in this study.

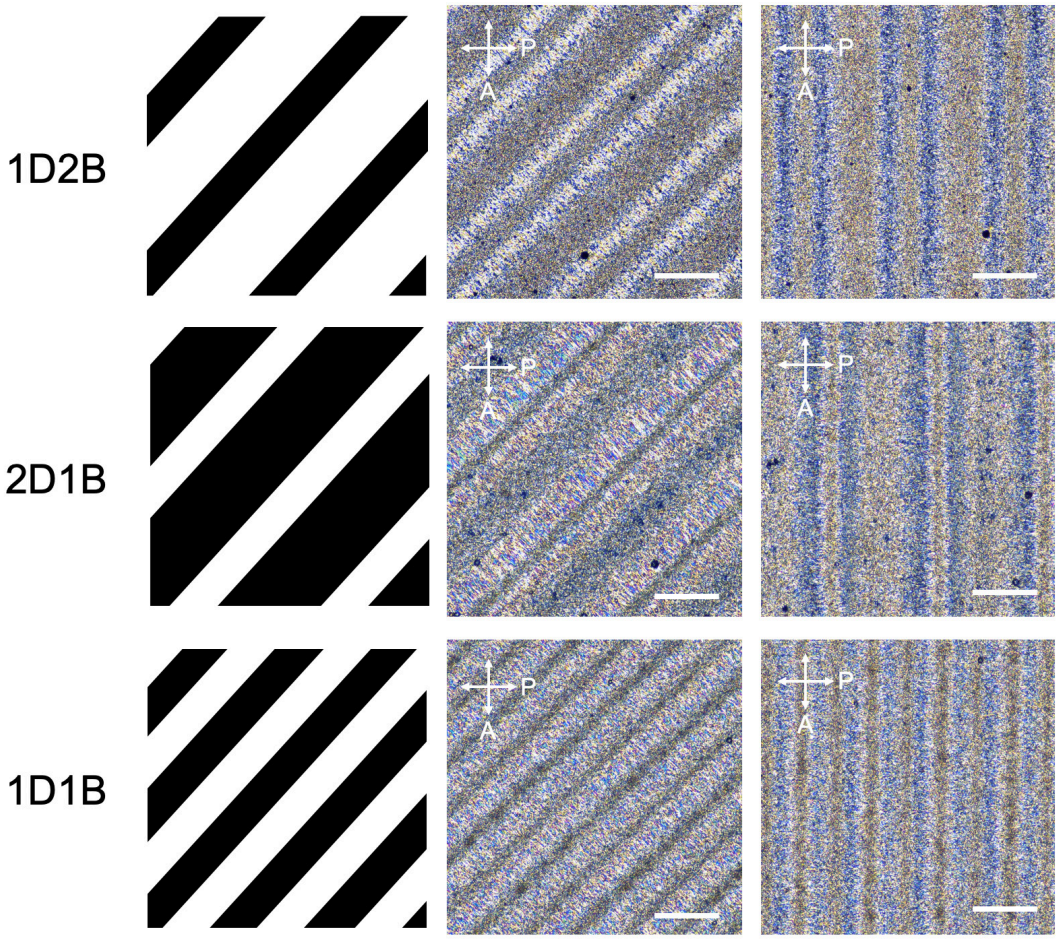


**Figure 2.** Left: Dark and bright striped patterns used to photopattern crystal orientation. Middle & right: POM images of photopatterned films between crossed polarizers (scale bars: 200 μm).

By introducing repeating aligned crystal patterns in the films, the direction of expansion of the films after melting can be controlled. The change in dimensions parallel and perpendicular to the pattern lines was measured after heating the films to 90˚C. For Control film, which was uniformly irradiated with unpatterned broadband light for 30 s, no significant difference between width and length change post-heating was observed ($p = 0.68$). All photopatterned films (1D2B, 2D1B, 1D1B) showed a significantly larger dimensional change in the direction perpendicular to the patterned lines (9–15%) than in the parallel direction (-2–1%) (1D2B, $p = 0.025$; 2D1B, p

=0.003; 1D1B. p=0.004). Among them, 1D1B showed the largest dimension change of around 15% (**Fig. 3a**). This increase in dimensional change of 1D1B was statistically significant when compared to the dimensional change of films processed with the other patterns. From this point on, the 1D1B pattern was used for further characterizations of the photopatterned films. When the films were heated to 90˚C, which is above the melting temperature, the crystals rapidly melted, and birefringence was not observed (**Fig. 3b**). After cooling the films to room temperature, the films crystallized again, but the regions of uniform birefringence were lost (**Fig. 3b**). As the aligned crystals melted and recrystallized, they reorganized into a more stable state, which was not in the aligned form.[32] **Fig. 3c** shows the dimension change of 1D1B films after heating and cooling for two cycles. The in-plane dimension perpendicular to the pattern lines increased significantly when heated and decreased slightly upon cooling due to crystallization. The dimensions parallel to the pattern lines slightly decreased upon heating as the film expanded significantly in the perpendicular direction. The dimension was further reduced when the film was crystallized on cooling. The dimensions of the film after the second cycle of heating and cooling were similar to the dimensions after the first cycle.

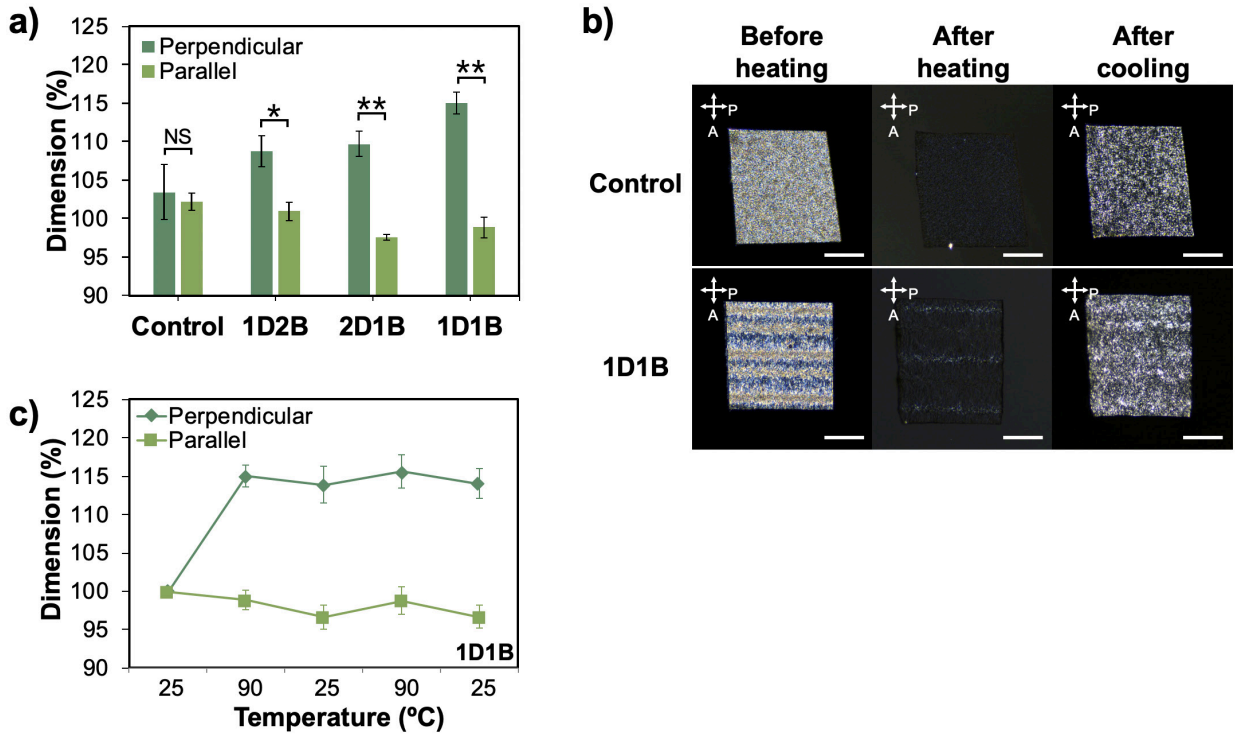


**Figure 3.** a) Dimension% of the polymer films with varying patterns perpendicular and parallel to the birefringent lines upon heating to 90˚C (n=3). (NS: not significant, * $p < 0.05$, ** $p < 0.01$) b) POM images of Control and 1D1B films before heating (25˚C), after heating (90˚C), and after cooling (25˚C) between crossed polarizers (scale bars: 200 μm). c) Dimension% for 1D1B films upon heating and cooling for two cycles (n=3).

The thermomechanical properties of the semicrystalline films are relatively unaffected by the presence of aligned crystal patterns. The thermal properties of the films were analyzed using differential scanning calorimetry (DSC). The melting temperatures of Control and 1D1B films were both around 59˚C, which indicates that photopatterning the films did not affect the thermal properties of the films (**Fig. 4a,b**). Mechanical properties were measured by dynamic mechanical analysis (DMA) using a strain sweep from 0.05% to 0.2% (**Figure S4**). 1D1B films were cut in

different angles of 0˚, 45˚, and 90˚ to the pattern lines to characterize the storage moduli with respect to the crystal orientation. For all of the samples, the strain remained in the elastic regime. The storage moduli for the samples were in the range of 210 – 310 MPa, which did not show a significant difference between Control and 1D1B films cut at different angles (**Fig. 4c**). This demonstrates the regions of aligned crystals did not significantly affect the elastic properties of the semicrystalline polymer films. The thermomechanical property of Control film was measured by DMA temperature sweep (**Fig. 4d**), and a large modulus change was observed between 60 – 63˚C due to the melting of crystallites, consistent with DSC results.

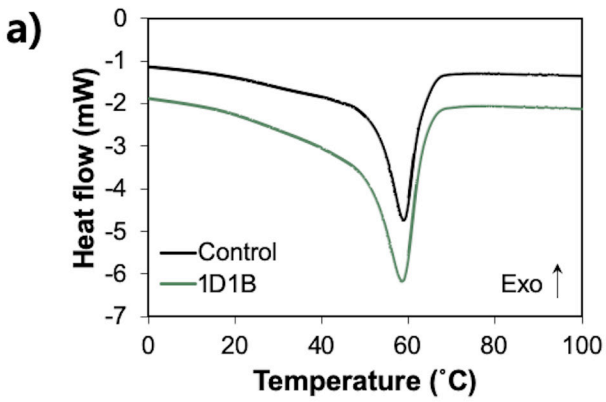


b)

| | Melting temperature ($T_m$ ; ˚C) | Enthalpy of melt (J/g) |
|---|---|---|
| Control | 58.9 ± 0.2 | 36.2 ± 3.8 |
| 1D1B | 58.6 ± 0.3 | 36.5 ± 1.9 |

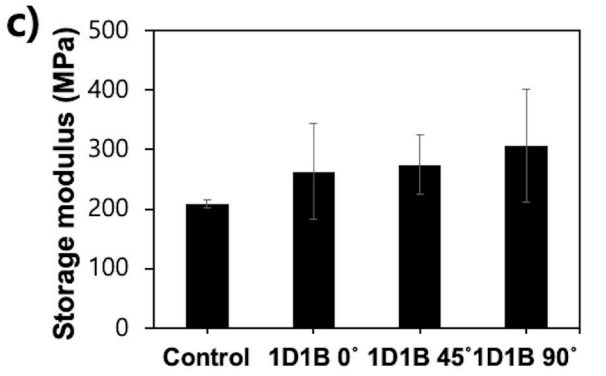


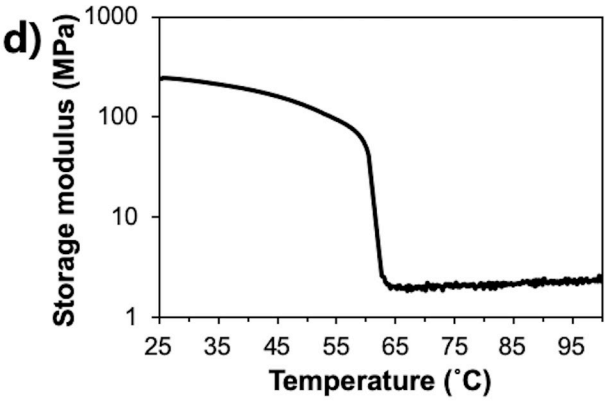


**Figure 4**. a) Representative thermograms of Control and 1D1B films measured by DSC. b) Melting temperature ($T_m$) and enthalpy of melt for Control and 1D1B films measured by DSC (n=3). c) Storage moduli of Control and 1D1B films cut at different angles at 0.1% strain (n=3). d) Representative thermomechanical spectrum of Control film measured using DMA temperature sweep at 0.2% strain with a 1 ˚C/min heating rate.

The orientation of the pattern in ribbons can be used to control the degree of twist upon thermal actuation. Control films were cut at five different angles (0˚, 20˚, 45˚, 70˚, and 90˚), and 1D1B films were cut at such that the orientation of the pattern and the short axis of the rectangular ribbon formed angles of 0˚, 20˚, 45˚, 70˚, and 90˚ (**Figure S5a)**. The rectangular ribbons (1 mm ×15 mm × 30 μm) were all flat at room temperature. Once heated to 90˚C in a silicone oil bath,

Control films bent towards the side nearest the projector light and the UV light during photopolymerization (**Figure S5b**). This bending can likely be attributed to differences in crosslink density between the two surfaces, which can make the surface nearer the crosslinking lights stiffer than the other. When undergoing melting, the expansion of the film can cause bending. The rapid formation of crystals and the associated stress at the surface facing light during crosslinking could potentially have contributed to the bending as well. The degree of bending according to different crosslinking times at the front and back of the films was analyzed by measuring the radius of curvature of heated film strips (**Figure S6**). Films were UV crosslinked for 10, 7.5, 5, and 2.5 min on the front side and 0, 2.5, 5, and 7.5 min on the backside, respectively. The mean radius of curvature increased with decreasing crosslinking time at the front and increasing crosslinking time at the back, which is due to the decrease of the gradients between two surfaces. For 1D1B films, expansion perpendicular to the photopatterned lines occurs as well as the bending upon heating. Therefore, as the 1D1B films are heated above the melting temperature, the films coiled in the direction perpendicular to the patterned lines, resulting in twisted coils with different angles (**Figure S5b**). Since Control films do not have any aligned crystal patterns, the cutting angle of the films did not affect the magnitude of coiling. Control films showed about 0.3 turns/mm with a helical angle close to 80˚. As the Control films are not anisotropic, the twist that is observed is likely due to self-contact of the bending film that restricts the film to coil at a helical angle of 90˚. For the 1D1B films, the number of turns/mm was the largest at the pattern angle of 0˚, which was similar to but slightly larger than that of the Control films. As the pattern angle increased, 1D1B films showed decreasing number of turns and increasing pitch (**Fig. 5a,b**). Helical angles for 1D1B films decreased from ~80˚ to ~30˚ up until the pattern angle of 70˚. When the pattern angle was 90˚, the helical angle could not be

defined since the 1D1B film showed slight bending instead of twisting (**Fig. 5c**). The results demonstrate that photopatterning crystal orientation can provide anisotropy in the shape change of the semicrystalline polymer films.

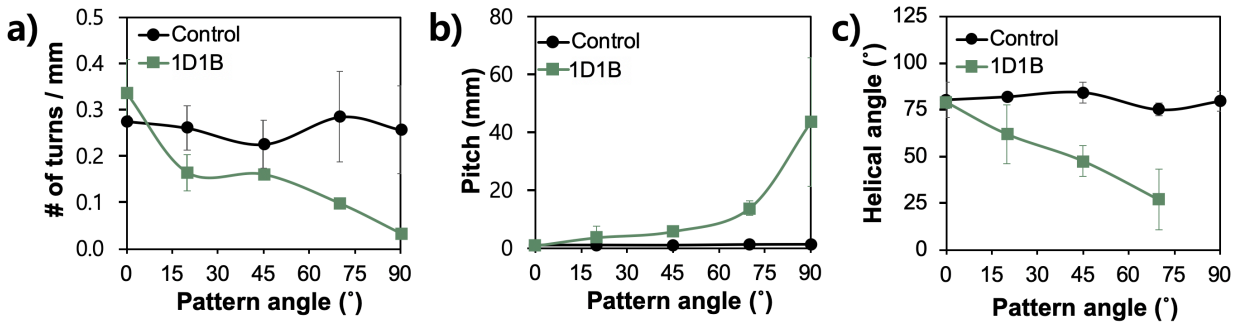


**Figure 5**. a) Number of turns per mm measured for Control and 1D1B ribbons with various pattern angles (n=3). b) Pitch measured for film samples at various pattern angles (n=3). c) Helical angles measured for film samples at various pattern angles (n=3).

By programming the dark and bright patterns in various orientations, more complex shapes upon heating can be achieved (**Fig. 6 and Figure S7**).[13,33,34] First, the 1D1B pattern was irradiated on the left half of the cell, while an inverted image of the 1D1B pattern was irradiated on the right half of the cell. The photopatterned film could actuate into a helical coil having a handedness inversion (**Figure S7**). To obtain a cone shape, a pattern having alternating dark and bright concentric circles was used. As the circumferences of the patterned circles shrink slightly while the corresponding radii expand, a cone shape could be achieved with a pointed apex, as has been proposed and observed in liquid crystal materials and hydrogels.[13,35,36] When a pattern consisting of radial lines was used, a flat circular film actuated into an 'anti-cone' shape or a saddle shape. The thermal actuation of the circular film elongated its circumferences and reduced the radii

slightly, which led to a buckling out of plane to minimize the bending and torsional energies, forming the 'anti-cone' shape.[35,36] A twisting flower shape could be established when each 'petal' of the flower had 45° striped lines. As each petal curled perpendicular to the patterned lines, five petals curled in five different directions. The results indicate that complex 3D shapes can be easily obtained by simply irradiating different dark and bright patterns during photopolymerization. Another unique property of this polymer system is that the roughness increases remarkably when heated above the melting temperature.[26] The root-mean-square ($R_q$) roughness of Control films increased from 0.3 μm to 1.0 μm after heating the films above the melting temperature (**Figure S2**). Using this polymer system, complex 3D structures with rough topography can be obtained, which is not easily achieved using previously reported techniques that require initial programming steps.[37–39]

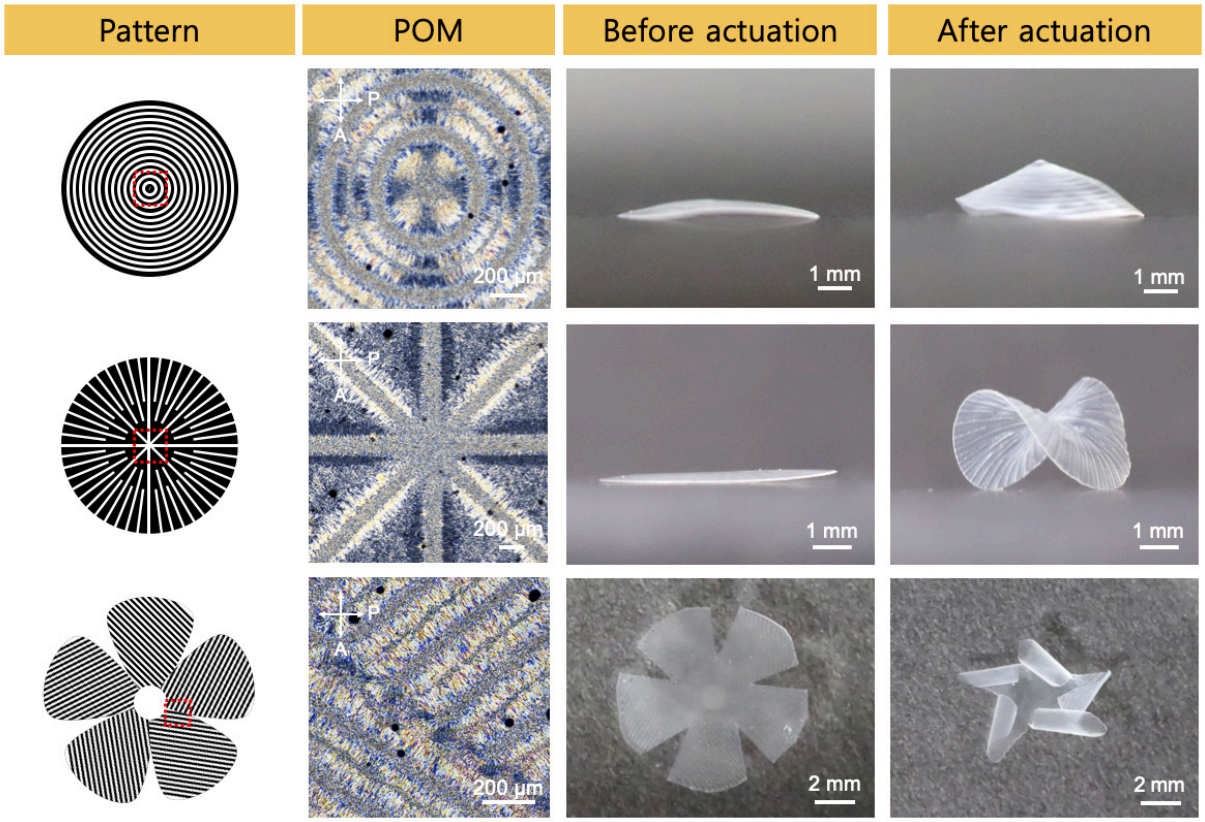


**Figure 6.** Left to right: Various patterns used for photoaligning crystal orientation of semicrystalline polymer films, POM images of photopatterned films using the patterns on the left between crossed polarizers (The areas shown in the POM images are indicated as red dotted boxes on the left patterns.), Images of hand-cut or biopsy-punched films prior to thermal actuation, Images of the films after thermal actuation in silicone oil at 90˚C.

To investigate the effect of polymerization temperature on the magnitude of shape change, films were photopatterned and polymerized at different temperatures of $T_m$ – 60˚C, $T_m$ – 35˚C, and $T_m$ – 10˚C. The polymerization temperatures were kept below the polymer's melting temperature to enable crystallization during photopolymerization.[26] Previously, we observed that the magnitude of roughness change on heating similar polymer films could be increased by increasing the temperature difference between the photopolymerization temperature and the melting temperature

of the network.[26] In addition, the crystallinity of the films increased with increasing the temperature difference between the photopolymerization and the melting temperature where X-ray diffraction was used to confirm crystallization in the materials.[26] The POM images of the films demonstrated that films polymerized at $T_m$ – 60˚C formed wider aligned crystalline regions compared to that of $T_m$ – 35˚C (**Fig. 7a**). Films polymerized at $T_m$ – 10˚C formed birefringent lines but did not show aligned crystals like the other two films. The lack of crystal orientation for films polymerized at $T_m$ – 10˚C suggests that the stress associated with concurrent crystallization orients the crystallites in the film. The diffusion of monomers should not be greatly influenced by this modest change in polymerization temperature, and therefore we do not expect it to be a primary mechanism of crystal alignment. Change in dimensions perpendicular to the crystal lines after heating decreased with the increasing polymerization temperature due to the reduced magnitude of aligned crystal formation (**Fig. 7b**).

By decreasing OTD:DAA ratio from 75:25 to 50:50, the melting temperature decreased from 59˚C to 42˚C (**Table S1**). Achieving melting temperature closer to body temperature can broaden the application range of this shape-morphing polymer system to biomedical fields. The films with 50:50 composition were photopatterned at $T_m$ – 35˚C with a 1D1B pattern, and the films showed aligned regions with aligned crystals (**Figure S8a**). Dimensional change in the perpendicular direction to the patterned lines was measured with increasing temperature for 75:25 and 50:50 1D1B films (**Fig. 7c**). The dimensions of the 75:25 film increased by 14% between 52˚C and 70˚C, while the dimensions of the 50:50 film increased by 8% between 34˚C and 56˚C. The smaller change in dimensions for 50:50 films compared to 75:25 films is likely due to a lower crystallinity of the 50:50 films as compared to the 75:25 films. Ribbons of 75:25 and 50:50 compositions

patterned at 45˚ of 1D1B pattern were heated in a silicone oil bath and imaged at intervals of 10˚C between 30˚C and 80˚C (**Figure S8b**). The 75:25 film was fully actuated and formed a helical coil between 60˚C and 70˚C, while the 50:50 film showed slight actuation at 50 ˚C and reached full actuation between 50˚C and 60˚C. The actuation temperature for 50:50 films (~55˚C) is slightly higher than the ideal actuation temperature (~40˚C) for biomedical device applications, which requires further modification on the chemical composition. The actuation temperature can be further lowered through many different ways such as by further decreasing OTD:DAA ratio, increasing PETMP crosslinker concentration, and using shorter chain dithiols than NDT (e.g., 1,6-hexanedithiol or 1,3-propanedithiol).[26]

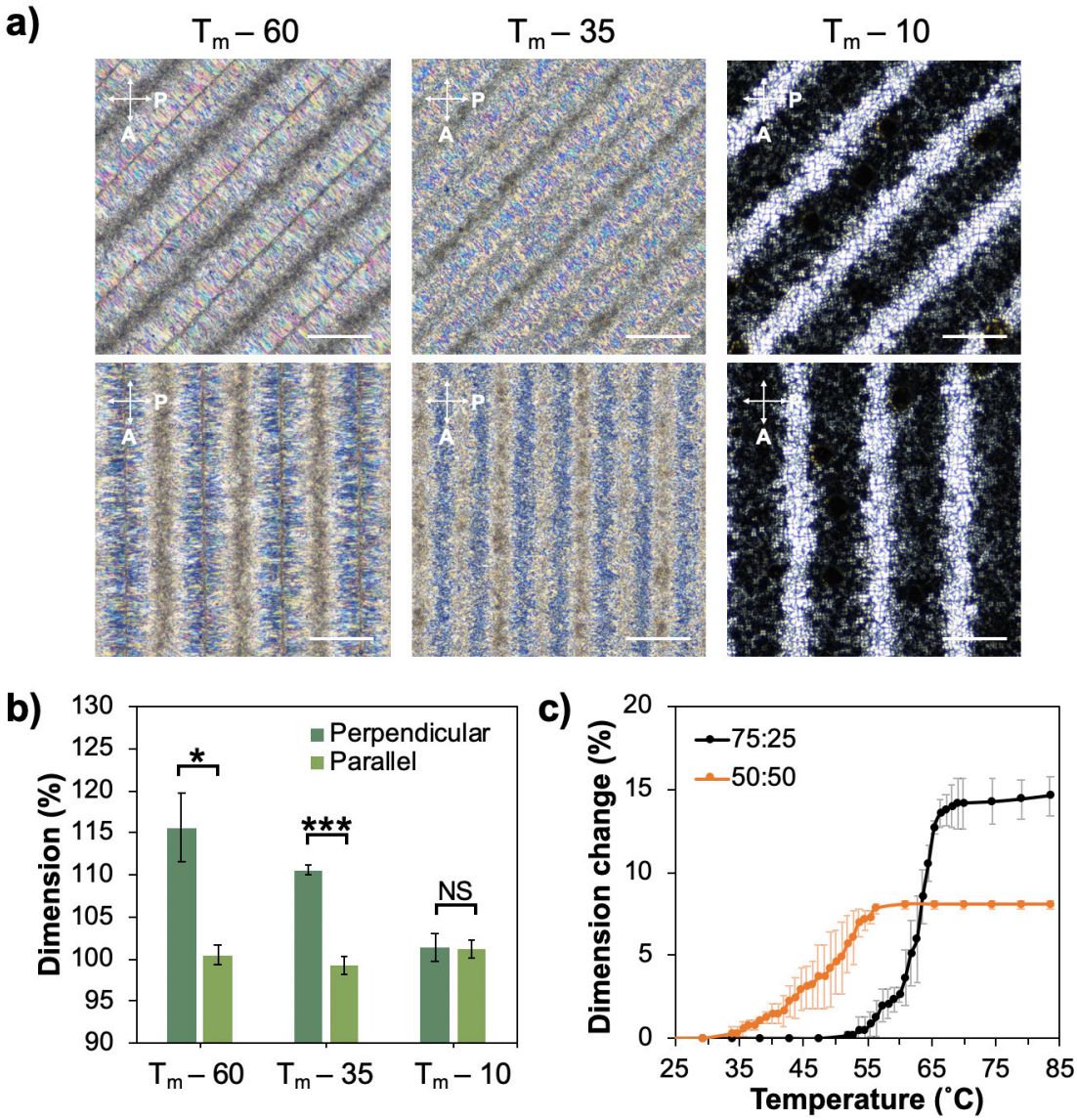


**Figure 7.** a) POM images of OTD:DAA = 75:25 composition films photopatterned with 1D1B pattern at three different polymerization temperatures ($T_m$ – 60 ˚C, $T_m$ – 35 ˚C and $T_m$ – 10 ˚C) using a dielectric mirror (Scale bars: 200 µm). b) Dimensions perpendicular and parallel to the crystal lines after thermal actuation of the films polymerized at three different temperatures (n=3). (NS: not significant, * $p < 0.05$, *** $p < 0.001$) c) Dimension change of 75:25 and 50:50 composition films perpendicular to the crystal lines with respect to temperature (n=3).

## 4. CONCLUSION

A new type of shape-morphing polymer was developed by photopatterning crystal orientation in semicrystalline polymer films by irradiating computer-generated patterns using a projector. This technique of photopatterning the crystal orientation provides a new route to programming shape morphing in polymeric materials. This method embeds the stimulus response in the film during processing in a scalable and non-mechanical manner. The resulting semicrystalline network possesses programmability, facile synthesis from simple thiol and alkene monomers, and robust mechanical properties. Furthermore, this approach is designed to be scalable for coatings and films and does not rely on directed self-assembly or 3D printing approaches to program shape change. The actuation temperature can be controlled by changing the chemical composition ratio. This shape-morphing polymer system, as well as the photopatterning technique used in the study, has the potential to be utilized in diverse applications from deployable electronics to morphing biomedical devices.

## ASSOCIATED CONTENT

The following files are available free of charge.

Supporting information (.doc): **Figure S1**. Schematic of the polymer network synthesized, **Figure S2**. Root-mean-square roughness ($R_q$) and 3D scans of Control films before and after heating, **Figure S3**. Average widths and the area % of the uniform birefringent lines, **Figure S4**. Representative strain sweeps of Control and 1D1B films using DMA, **Figure S5**. Schematic of a coiled ribbon and the metrics used for helical shape analysis, Images of heated Control and 1D1B ribbons cut at various angles, **Figure S6**. Radius of curvature measured for 75:25 films with varying crosslinking times, **Figure S7**. Actuation of a flat photopatterned film into a helical

coil with a handedness inversion, **Figure S8**. POM images of OTD:DAA = 50:50 composition films polymerized at $T_m$ – 35˚C, Images of ribbons of 75:25 and 50:50 composition undergoing thermal actuation in silicon oil at different temperatures, **Table S1**. DSC analysis of OTD:DAA = 50:50 composition films.

AUTHOR INFORMATION

**Corresponding Author**

*Taylor H. Ware.

taylor.ware@tamu.edu

**Author Contributions**

The manuscript was written through contributions of all authors. All authors have given approval to the final version of the manuscript.

**Funding Sources**

This material is based upon work supported by the National Science Foundation under Grant No. DMR 2041671.

ACKNOWLEDGMENT

The authors would like to thank Tyler Corazao for his help on some experiments. The authors also would like to acknowledge AggieFab Nanofabrication Facility at Texas A&M University for their surface analysis using a surface profiler and an optical profilometer.

## ABBREVIATIONS

OTD, 1,7-octadiene; DAA, diallyl adipate; PETMP, pentaerythritol tetrakis(3-mercaptopropionate); NDT, 1,9-nonanedithiol; IPA, isopropyl alcohol; I-819, bis(2,4,6-trimethylbenzoyl)phenylphosphine oxide; RO, reverse osmosis; POM, polarizing optical microscope; DSC, differential scanning calorimetry; DMA, dynamic mechanical analysis.

## REFERENCES

(1) Verpaalen, R. C.; Pilz da Cunha, M.; Engels, T. A.; Debije, M. G.; Schenning, A. P. Liquid Crystal Networks on Thermoplastics: Reprogrammable Photo-responsive Actuators. *Angew. Chem. Int. Ed.* **2020**, *59* (11), 4532–4536.
(2) Li, Y.; Chen, H.; Liu, D.; Wang, W.; Liu, Y.; Zhou, S. PH-Responsive Shape Memory Poly (Ethylene Glycol)–Poly (ε-Caprolactone)-Based Polyurethane/Cellulose Nanocrystals Nanocomposite. *ACS Appl. Mater. Interfaces* **2015**, *7* (23), 12988–12999.
(3) Okuzaki, H.; Funasaka, K. Electro-Responsive Polypyrrole Film Based on Reversible Sorption of Water Vapor. *Synth. Met.* **2000**, *108* (2), 127–131.
(4) Jang, L. K.; Fletcher, G. K.; Monroe, M. B. B.; Maitland, D. J. Biodegradable Shape Memory Polymer Foams with Appropriate Thermal Properties for Hemostatic Applications. *J. Biomed. Mater. Res. A* **2020**, *108* (6), 1281–1294. https://doi.org/10.1002/jbm.a.36901.
(5) Filipcsei, G.; Csetneki, I.; Szilágyi, A.; Zrínyi, M. Magnetic Field-Responsive Smart Polymer Composites. *Oligomers-Polym. Compos.-Mol. Imprinting* **2007**, 137–189.
(6) Kerry, J.; Butler, P. *Smart Packaging Technologies for Fast Moving Consumer Goods*; John Wiley & Sons, 2008.
(7) Cho, K. H.; Song, M. G.; Jung, H.; Park, J.; Moon, H.; Koo, J. C.; Nam, J.-D.; Choi, H. R. A Robotic Finger Driven by Twisted and Coiled Polymer Actuator; International Society for Optics and Photonics, 2016; Vol. 9798, p 97981J.
(8) Takashima, K.; Rossiter, J.; Mukai, T. McKibben Artificial Muscle Using Shape-Memory Polymer. *Sens. Actuators Phys.* **2010**, *164* (1–2), 116–124.
(9) Yakacki, C. M.; Shandas, R.; Lanning, C.; Rech, B.; Eckstein, A.; Gall, K. Unconstrained Recovery Characterization of Shape-Memory Polymer Networks for Cardiovascular Applications. *Biomaterials* **2007**, *28* (14), 2255–2263.

(10) Zhao, Q.; Wang, J.; Cui, H.; Chen, H.; Wang, Y.; Du, X. Programmed Shape-morphing Scaffolds Enabling Facile 3D Endothelialization. *Adv. Funct. Mater.* **2018**, *28* (29), 1801027.
(11) Liu, C.; Qin, H.; Mather, P. Review of Progress in Shape-Memory Polymers. *J. Mater. Chem.* **2007**, *17* (16), 1543–1558.
(12) Klein, Y.; Efrati, E.; Sharon, E. Shaping of Elastic Sheets by Prescription of Non-Euclidean Metrics. *Science* **2007**, *315* (5815), 1116–1120.
(13) Gladman, A. S.; Matsumoto, E. A.; Nuzzo, R. G.; Mahadevan, L.; Lewis, J. A. Biomimetic 4D Printing. *Nat. Mater.* **2016**, *15* (4), 413–418.
(14) Kim, J.; Hanna, J. A.; Hayward, R. C.; Santangelo, C. D. Thermally Responsive Rolling of Thin Gel Strips with Discrete Variations in Swelling. *Soft Matter* **2012**, *8* (8), 2375–2381.
(15) Ware, T. H.; McConney, M. E.; Wie, J. J.; Tondiglia, V. P.; White, T. J. Voxelated Liquid Crystal Elastomers. *Science* **2015**, *347* (6225), 982–984.
(16) White, T. J.; Broer, D. J. Programmable and Adaptive Mechanics with Liquid Crystal Polymer Networks and Elastomers. *Nat. Mater.* **2015**, *14* (11), 1087–1098.
(17) Liu, D.; Broer, D. J. Liquid Crystal Polymer Networks: Preparation, Properties, and Applications of Films with Patterned Molecular Alignment. *Langmuir* **2014**, *30* (45), 13499–13509.
(18) Xie, T. Recent Advances in Polymer Shape Memory. *Polymer* **2011**, *52* (22), 4985–5000.
(19) Lendlein, A.; Kelch, S. Shape-Memory Polymers. *Angew. Chem. Int. Ed.* **2002**, *41* (12), 2034–2057. https://doi.org/10.1002/1521-3773(20020617)41:12<2034::AID-ANIE2034>3.0.CO;2-M.
(20) Behl, M.; Razzaq, M. Y.; Lendlein, A. Multifunctional Shape-Memory Polymers. *Adv. Mater.* **2010**, *22* (31), 3388–3410. https://doi.org/10.1002/adma.200904447.
(21) Liu, Y.; Genzer, J.; Dickey, M. D. "2D or Not 2D": Shape-Programming Polymer Sheets. *Prog. Polym. Sci.* **2016**, *52*, 79–106. https://doi.org/10.1016/j.progpolymsci.2015.09.001.
(22) Liu, Y.; Boyles, J. K.; Genzer, J.; Dickey, M. D. Self-Folding of Polymer Sheets Using Local Light Absorption. *Soft Matter* **2012**, *8* (6), 1764–1769.
(23) Liu, Y.; Miskiewicz, M.; Escuti, M. J.; Genzer, J.; Dickey, M. D. Three-Dimensional Folding of Pre-Strained Polymer Sheets via Absorption of Laser Light. *J. Appl. Phys.* **2014**, *115* (20), 204911.
(24) Mao, Y.; Yu, K.; Isakov, M. S.; Wu, J.; Dunn, M. L.; Qi, H. J. Sequential Self-Folding Structures by 3D Printed Digital Shape Memory Polymers. *Sci. Rep.* **2015**, *5* (1), 1–12.
(25) Yu, K.; Ritchie, A.; Mao, Y.; Dunn, M. L.; Qi, H. J. Controlled Sequential Shape Changing Components by 3D Printing of Shape Memory Polymer Multimaterials. *IUTAM Symp. Mech. Soft Act. Mater.* **2015**, *12*, 193–203. https://doi.org/10.1016/j.piutam.2014.12.021.
(26) Abdelrahman, M. K.; Kim, H.; Maeng, J.; Ondrusek, P.; Ware, T. H. Emergent Surface Topography Enabled by Concurrent Crystallization and Polymerization. *Macromolecules* **2020**, *53* (7), 2388–2395. https://doi.org/10.1021/acs.macromol.9b02703.
(27) Childress, K. K.; Alim, M. D.; Hernandez, J. J.; Stansbury, J. W.; Bowman, C. N. Additive Manufacture of Lightly Crosslinked Semicrystalline Thiol–Enes for Enhanced Mechanical Performance. *Polym. Chem.* **2020**, *11* (1), 39–46.
(28) Hisano, K.; Kurata, Y.; Aizawa, M.; Ishizu, M.; Sasaki, T.; Shishido, A. Alignment Layer-Free Molecular Ordering Induced by Masked Photopolymerization with Non-Polarized Light. *Appl. Phys. Express* **2016**, *9* (7), 072601.

(29) Sutherland, R.; Natarajan, L.; Tondiglia, V.; Bunning, T. Bragg Gratings in an Acrylate Polymer Consisting of Periodic Polymer-Dispersed Liquid-Crystal Planes. *Chem. Mater.* **1993**, *5* (10), 1533–1538.
(30) Sánchez, C.; de Gans, B.; Kozodaev, D.; Alexeev, A.; Escuti, M. J.; Van Heesch, C.; Bel, T.; Schubert, U. S.; Bastiaansen, C. W.; Broer, D. J. Photoembossing of Periodic Relief Structures Using Polymerization-induced Diffusion: A Combinatorial Study. *Adv. Mater.* **2005**, *17* (21), 2567–2571.
(31) Hisano, K.; Aizawa, M.; Ishizu, M.; Kurata, Y.; Nakano, W.; Akamatsu, N.; Barrett, C. J.; Shishido, A. Scanning Wave Photopolymerization Enables Dye-Free Alignment Patterning of Liquid Crystals. *Sci. Adv.* **2017**, *3* (11), e1701610.
(32) Wunderlich, B. The Melting of Defect Polymer Crystals. *Polymer* **1964**, *5*, 611–624.
(33) McConney, M. E.; Martinez, A.; Tondiglia, V. P.; Lee, K. M.; Langley, D.; Smalyukh, I. I.; White, T. J. Topography from Topology: Photoinduced Surface Features Generated in Liquid Crystal Polymer Networks. *Adv. Mater.* **2013**, *25* (41), 5880–5885.
(34) Kotikian, A.; Truby, R. L.; Boley, J. W.; White, T. J.; Lewis, J. A. 3D Printing of Liquid Crystal Elastomeric Actuators with Spatially Programed Nematic Order. *Adv. Mater.* **2018**, *30* (10), 1706164.
(35) Modes, C.; Bhattacharya, K.; Warner, M. Gaussian Curvature from Flat Elastica Sheets. *Proc. R. Soc. Math. Phys. Eng. Sci.* **2011**, *467* (2128), 1121–1140.
(36) de Haan, L. T.; Sánchez-Somolinos, C.; Bastiaansen, C. M.; Schenning, A. P.; Broer, D. J. Engineering of Complex Order and the Macroscopic Deformation of Liquid Crystal Polymer Networks. *Angew. Chem.* **2012**, *124* (50), 12637–12640.
(37) Lee, E. M.; Smith, K.; Gall, K.; Boyan, B. D.; Schwartz, Z. Change in Surface Roughness by Dynamic Shape-Memory Acrylate Networks Enhances Osteoblast Differentiation. *Biomaterials* **2016**, *110*, 34–44.
(38) Thapa, A.; Miller, D. C.; Webster, T. J.; Haberstroh, K. M. Nano-Structured Polymers Enhance Bladder Smooth Muscle Cell Function. *Biomaterials* **2003**, *24* (17), 2915–2926. https://doi.org/10.1016/S0142-9612(03)00123-6.
(39) Nickmans, K.; van der Heijden, D. A.; Schenning, A. P. Photonic Shape Memory Chiral Nematic Polymer Coatings with Changing Surface Topography and Color. *Adv. Opt. Mater.* **2019**, *7* (19), 1900592.

For Table of Contents Only